IEEE Access
Multidisciplinary | Rapid Review | Open Access Journal

Received May 21, 2021, accepted June 2, 2021, date of publication June 11, 2021, date of current version June 21, 2021.

Digital Object Identifier 10.1109/ACCESS.2021.3088458

Lead-Free Piezoelectric Composite With Lithium Niobate and Barium Titanate Fabricated by Interdigital Pair Bonding Technique

KYUNGMIN KIM[1], (Graduate Student Member, IEEE), JINHEE YOO[2], (Graduate Student Member, IEEE), HAE GYUN LIM[3], MINA LEE[1], SUNG-MIN PARK[1,2,4,5], (Member, IEEE), AND HYUNG HAM KIM[1,2,4], (Member, IEEE)

[1]Department of Convergence IT Engineering, Pohang University of Science and Technology (POSTECH), Pohang 37673, Republic of Korea
[2]School of Interdisciplinary Bioscience and Bioengineering, Pohang University of Science and Technology (POSTECH), Pohang 37673, Republic of Korea
[3]Department of Biomedical Engineering, Pukyong National University, Busan 48513, Republic of Korea
[4]Department of Electrical Engineering, Pohang University of Science and Technology (POSTECH), Pohang 37673, Republic of Korea
[5]Department of Mechanical Engineering, Pohang University of Science and Technology (POSTECH), Pohang 37673, Republic of Korea

Corresponding author: Hyung Ham Kim (david.kim@postech.ac.kr)

This work was supported in part by the Basic Science Research Program through the National Research Foundation of Korea (NRF) funded by the Ministry of Education under Grant 2020R1A6A103047902, in part by the NRF grant funded by the Ministry of Science and Information and Communications Technology (ICT) under Grant 2019R1A2C2010484, and in part by the ICT Creative Consilience program supervised by the Institute for Information & Communications Technology Planning & Evaluation (IITP) under Grant IITP-2020-2011-1-00783.

ABSTRACT Since 2003, when the European Union (E.U.) announced the restriction of hazardous substances (RoHS), multiple efforts have been made to replace lead zirconate titanate (PZT) based piezoelectric materials. However, despite these efforts, very few PZT alternatives have been found. The Lithium niobate (LN) is one such lead-free piezoelectric material often used in acoustic applications due to its high signal generation efficiency, high curie temperature, and high mechanical Q factor. However, LN is not suitable for miniaturized applications because of its low dielectric constant and high electrical impedance. In this paper, we aim to address the problem of the low-dielectric constant of LN while avoiding hazardous PZT material. We propose to utilize 1-3 composites structure with LN and barium titanate (BT), which has a high dielectric constant while controlling acoustic properties such as density, dielectric constant, sound velocity. We also developed new LN-BT modeling to design piezoelectric composite with interdigital pair bonding (IPB) technique, based on previous PZT-polymer 1-3 composite modeling. We verified that the composite components are lead-free by examining with the scanning electron microscope (SEM) with energy dispersive X-ray spectroscopy (EDS) and X-ray diffraction (XRD). This proposed lead-free composite with high-dielectric and lower electrical impedance is better suited for miniaturized applications.

INDEX TERMS Lithium niobate, barium titanate, piezoelectric composite material, constitutive relationship, interdigital pair bonding.

I. INTRODUCTION

Since the early 2000s, legislations have been put worldwide to restrict the use of certain Hazardous substances in Electrical and Electronic Equipment (RoHS) such as lead, cadmium, or mercury [1]. Despite these regulations, the medical industry uses restricted materials through the RoHS exemption clause (annex III and IV) due to a lack of alternatives. For example, medical ultrasound imaging and the therapeutic system still manufacture transducers from lead-included material such as Lead Zirconate Titanate (PZT). However, once high-performance lead-free piezoelectric materials become available, RoHS exemptions could potentially be eliminated, thus eliminating the use of hazardous material. Researchers have been actively searching high-performing lead-free piezoelectric materials for clinical applications, such as Barium Titanate (BT, $BaTiO_3$), Potassium Sodium Niobate ($K_xN_{(1-x)}N$),

The associate editor coordinating the review of this manuscript and approving it for publication was Yingxiang Liu.

TABLE 1. Properties of piezoelectric materials [3], [8]–[10].

	PZT	KNN	LN
Curie Temperature [T_c (°C)]	225	410	1150
piezoelectric coefficient [d_{33} ($C/N\times10^{-12}$)]	650	90	6
Dielectric constant - Strain [ε_{33}^S]	1200	190	27.9
Dielectric constant - Stress [ε_{33}^T]	3800	292	28.7
Electromechanical coupling coefficient [k_t]	0.55	0.5	0.485
Mechanical Q factor [Q_m]	50	1500	10000

or a pseudobinary ferroelectric system (1-x)$Ba(Zr_{0.2}Ti_{0.8})O_3$-x$(Ba_{0.7}Ca_{0.3})TiO_3$ (BZT-100xBCT) [2]–[5]. Of these, KNN has a high dielectric constant (ε), a high piezoelectric coefficient (d_{33}), and a high electromechanical coupling coefficient (k_t) compared to other lead-free piezoelectric materials [5]–[8]. Thus, KNN has been well received by the industry and researchers alike and has been applied to many applications such as piezoelectric motor, energy harvesting sensors, or medical acoustic transducers. However, KNN has poor temperature stability and insufficient densification, which are the limiting factors for stable fabrication. For these reasons, the wide use of KNN is still limited [9].

The Lithium Niobate (LN, $LiNbO_3$) is a ferroelectric material and has been in use for acoustic applications since its ferroelectric properties were discovered in 1949 [10]. LN is widely used in various research and industrial applications [11]–[13]. The LN has not only high productivity but also good k_t values, high Curie temperature (T_c), and high mechanical quality factor (Q_m) [14], [15]. The high Q_m value allows the transmit sensitivity of the ultrasound transducer to be improved for specific frequency bands. The high Curie temperature makes it possible for it to be used in extreme conditions requiring exposure to high-temperature environments such as nondestructive testing (NDT) of the heated metal or the system that require a high process temperature [16]. However, the main limitation of LN is its low dielectric constant characteristic, which causes high electrical impedance when the material is miniaturized. As a result, it is challenging to use LN for miniaturization applications such as small piezoelectric sensors, multi-layer ceramic capacitors, medical array transducers, etc. Thus, if LN can solve low dielectric constant while keeping its numerous advantages, it could become an alternative high-performance, lead-free material that can replace PZT.

Various methods have been studied to improve the piezoelectric performance of materials, and the representative methods are to use composite structures combining multiple materials with specific geometrical arrangements such as 0-3, 2-2, and 1-3 [17]–[20]. Combining LN and BT leads to a higher dielectric constant composite. In this study, we aim to overcome the low-dielectric shortcoming of LN by proposing an LN-BT composite using a new 1-3 composite modeling and interdigital pair bonding (IPB) fabrication method.

We also proposed new modeling suitable for the LN-BT composite and compared the simulated and measured values to validate the model. The previously proposed model to evaluate the 1-3 composite performance using PZT and polymer cannot be used for LN-BT composite since their crystal structures have different constitutive equations [20], [21]. The materials we used, LN and BT, have trigonal and tetragonal structures at room temperature, respectively, and a new modeling suitable for the crystal structure of LN and BT is needed [22], [23].

For the fabrication of the proposed LN-BT 1-3 composite, we used the IPB method with a solid LN plate and a solid BT plate, enabling the composite to have a high dielectric constant of BT compared to the dice-and-fill method [24], [25]. Since the dice-and-fill method requires high-temperature and high-pressure processes, those conditions generally lead to an adverse effect on piezoelectric properties, making it difficult to achieve a high dielectric constant. We prepared multiple samples with various volume fraction ratios and measured the electrical impedance using an impedance analyzer. We also obtained pictures of finished composites by a scanning electron microscope (SEM) and confirmed it has a perovskite structure. In addition, we confirmed that the composite is lead-free using X-ray diffraction (XRD) and energy dispersive X-ray spectroscopy (EDS). In the following few sections, we will present details of our design along with results and discussion.

II. MATERIALS AND METHODS

The new model to predict the characteristics of a piezoelectric composite is based on the constitutive equation matrix of LN-BT. The model also verifies the modified composite material fabrication method, which guarantees a high dielectric constant of the finished composite.

A. LN BASED COMPOSITE MODELING

The structure of the LN has threefold rotational symmetry about its c axis and three mirror planes, and it is included in the 3m point group (space group R3c) of the crystallographic classification [23]. LN is generally classified into X-cut, Y-cut, and Z-cut according to the cutting axis, and it is expressed as $(2\bar{1}\bar{1}0)$, $(1\bar{1}00)$, and (0001) respectively by Miller-Bravais indices. Since the Y-cut LN has a large amount of surface charge compared to Z-cut and X-cut, it has a higher k_t value and can be used for an ultrasound actuator [26], [27]. However, Y-cut LN does not have a homogeneous structure, and the phase of Y-cut LN crystal generally has a

(a)

$$\begin{pmatrix} T_1 \\ T_2 \\ T_3 \\ T_4 \\ T_5 \\ T_6 \\ D_1 \\ D_2 \\ D_3 \end{pmatrix} = \left(\begin{array}{cccccc|ccc} C_{11} & C_{12} & C_{13} & C_{14} & 0 & 0 & 0 & -e_{22} & e_{31} \\ C_{12} & C_{11} & C_{13} & -C_{14} & 0 & 0 & 0 & e_{22} & e_{31} \\ C_{13} & C_{13} & C_{33} & 0 & 0 & 0 & 0 & 0 & e_{33} \\ C_{14} & -C_{14} & 0 & C_{44} & 0 & 0 & 0 & e_{15} & 0 \\ 0 & 0 & 0 & 0 & 0 & C_{14} & e_{15} & 0 & 0 \\ 0 & 0 & 0 & 0 & C_{14} & C_{66} & -e_{22} & 0 & 0 \\ \hline 0 & 0 & 0 & 0 & e_{15} & -e_{22} & \varepsilon_{11} & 0 & 0 \\ -e_{22} & e_{22} & 0 & e_{15} & 0 & 0 & 0 & \varepsilon_{11} & 0 \\ e_{31} & e_{31} & e_{33} & 0 & 0 & 0 & 0 & 0 & \varepsilon_{33} \end{array}\right) \begin{pmatrix} S_1 \\ S_2 \\ S_3 \\ S_4 \\ S_5 \\ S_6 \\ E_1 \\ E_2 \\ E_3 \end{pmatrix}$$

(b)

$$\begin{pmatrix} T_1 \\ T_2 \\ T_3 \\ T_4 \\ T_5 \\ T_6 \\ D_1 \\ D_2 \\ D_3 \end{pmatrix} = \left(\begin{array}{cccccc|ccc} C_{11} & C_{12} & C_{13} & 0 & 0 & 0 & 0 & 0 & e_{31} \\ C_{12} & C_{11} & C_{13} & 0 & 0 & 0 & 0 & 0 & e_{31} \\ C_{13} & C_{13} & C_{33} & 0 & 0 & 0 & 0 & 0 & e_{33} \\ 0 & 0 & 0 & C_{44} & 0 & 0 & 0 & e_{15} & 0 \\ 0 & 0 & 0 & 0 & C_{44} & 0 & e_{15} & 0 & 0 \\ 0 & 0 & 0 & 0 & 0 & C_{44} & 0 & 0 & 0 \\ \hline 0 & 0 & 0 & 0 & e_{15} & 0 & \varepsilon_{11} & 0 & 0 \\ 0 & 0 & 0 & e_{15} & 0 & 0 & 0 & \varepsilon_{11} & 0 \\ e_{31} & e_{31} & e_{33} & 0 & 0 & 0 & 0 & 0 & \varepsilon_{33} \end{array}\right) \begin{pmatrix} S_1 \\ S_2 \\ S_3 \\ S_4 \\ S_5 \\ S_6 \\ E_1 \\ E_2 \\ E_3 \end{pmatrix}$$

FIGURE 1. The constitutive equation matrix for (a) tetragonal structure, BT and (b) a trigonal structure, LN. C, e, and ε are elastic stiffness constant, piezoelectric coefficient, and dielectric constant, respectively.

trigonal structure at room temperature. Thus, the previous ceramic-based composite modeling, which uses the tetragonal structure of ceramic and the constitutive equation of polymer, was not suitable for LN-BT composite. The Y-cut LN composite needs new modeling using a different constitutive equation matrix for the simulation. Here we propose new modeling for Y-cut LN using the ceramic-based composite model and effective medium theory [18], [21].

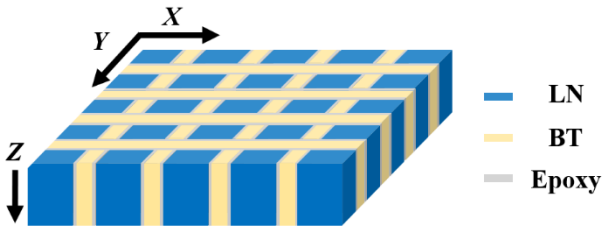

FIGURE 2. The geometry and connectivity of a 1-3 composite sample. Blue, yellow, and gray were LN, BT, and epoxy, respectively.

The new modeling applies to a 1-3 piezoelectric composite vibrating in the thickness mode. The geometry and connectivity of a designed 1-3 composite are shown in Fig. 2. The composite plate is on the X-Y plane, and the LN pillars are aligned along Z-axis. We used a constitutive equation matrix to relate stress (T), strain (S), electric displacement (D) and electric field (E) expressed in the Cartesian coordinate system [28], [29]. We have made the following assumptions in designing the model and are based on the previous modeling practices [18], [21].

Assumption 1: The stress, strain, and electric field are expressed independently on the two materials, LN and BT. We consider total stress (T) and total strain (S) divided into stress (T^L) and strain (S^L) for LN, and stress (T^C) and strain (S^C) for BT.

Assumption 2: The composite sample is large and sufficiently thin.

Assumption 3: The same voltage is applied to LN and BT parts. We assume that the electric fields of LN and BT are the same if the thickness of the sample and applied voltages of LN and BT are the same.

Assumption 4: Electrodes are deposited on both sides of the plate in a direction parallel to the composite plate. We assume that the electric fields (E_1, E_2) in the X and Y directions are zero except the electric field (E_3) in the vertical direction of the electrode.

Assumption 5: The rods of LN and BT are connected by epoxy and are assumed to oscillate at the same time. Even though the magnitude of vibration is different depending on the hardness and density of the material, it is assumed the same because of the strong epoxy binding between the LN and BT parts. We assumed that the strain in the vibration direction of LN (S_3^L) and BT (S_3^C) are the same.

$$\begin{aligned} T_1^L &= C_{11}^L S_1^L + C_{12}^L S_2^L + C_{13}^L S_3 + C_{14}^L S_4^L - e_{31}^L E_3 \\ T_2^L &= C_{12}^L S_1^L + C_{11}^L S_2^L + C_{13}^L S_3 - C_{14}^L S_4^L - e_{31}^L E_3 \\ T_3^L &= C_{13}^L S_1^L + C_{13}^L S_2^L + C_{33}^L S_3 - e_{33}^L E_3 \\ D_3^L &= e_{31}^L S_1^L + e_{31}^L S_2^L + e_{33}^L S_3 + \varepsilon_{33}^L E_3 \end{aligned} \tag{1}$$

$$\begin{aligned} T_1^C &= C_{11}^C S_1^C + C_{12}^C S_2^C + C_{13}^C S_3 - e_{31}^C E_3 \\ T_2^C &= C_{12}^C S_1^C + C_{11}^C S_2^C + C_{13}^C S_3 - e_{31}^C E_3 \\ T_3^C &= C_{13}^C S_1^C + C_{13}^C S_2^C + C_{33}^C S_3 + e_{33}^C E_3 \\ D_3^C &= e_{31}^C S_1^C + e_{31}^C S_2^C + e_{31}^C S_3 + \varepsilon_{11}^C E_3 \end{aligned} \tag{2}$$

Using Fig. 1 and assumptions 1-5, we reorganized constitutive equations (1) and (2) for LN (superscript L) and BT (superscript C), respectively.

Assumption 6: We assumed that the stresses of LN and BT are the same in each direction of X and Y, and there is no deformation because it is compensated by the interaction of the strain of LN and BT.

Assumption 6 is expressed as equation (3), where v and v' are the volume fraction ratio of LN and BT, respectively.

$$\begin{aligned} T_1^C &= T_1^L = T_1, T_2^C = T_2^L = T_2 \\ S_1 &= vS_1{}^C + v'S_1{}^L = 0, S_2 = vS_2{}^C + v'S_2{}^L = 0 \\ v' &= 1 - v \end{aligned} \tag{3}$$

Substituting equations (1) and (2) into equation (3), the relationship between S_1 and S_2 of LN and BT can be derived and the result is shown in equation (4). The equations to express the stress and displacement in the vibration direction, equations (5) and (6), can be obtained by substituting equation (4) into T_3^C and T_3^L of equations (1) and (2) and are shown below:

$$S_1^L + S_2^L = \frac{v' \left\{2\left(C_{13}^C - C_{13}^L\right) S_3 - 2\left(e_{31}^C - e_{31}^L\right) E_3\right\}}{v' C_{11}^L + v C_{11}^C + v C_{12}^C + v' C_{12}^L}$$

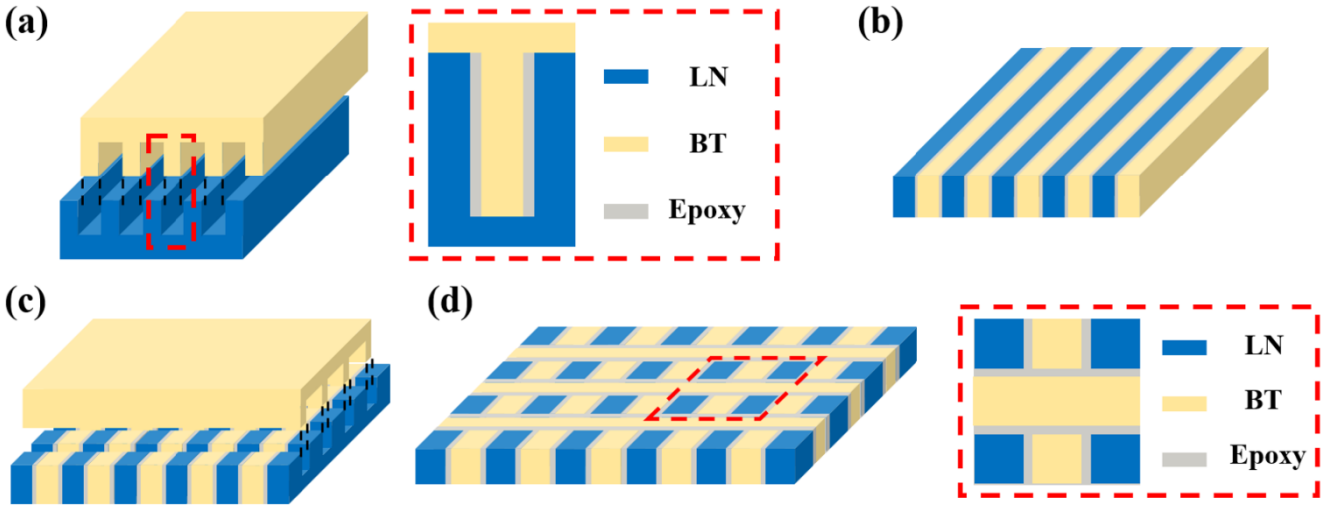

FIGURE 3. The image for interdigital pair bonding fabrication process and structure. (a) interdigital diced materials and combination process, (b) after the lapping process for the composite material, (c) repeat the process (a) and (b) vertically, and (d) 1-3 composite structure image fabricated by IPB.

$$S_1^C + S_2^C = \frac{-v\left\{2\left(C_{13}^C - C_{13}^L\right)S_3 - 2\left(e_{31}^C - e_{31}^L\right)E_3\right\}}{v'C_{11}^L + vC_{11}^C + vC_{12}^C + v'C_{12}^L} \tag{4}$$

$$\overline{T_3} = \left[\frac{2vv'(C_{13}^C - C_{13}^L)(C_{13}^L - C_{13}^C)}{v'C_{11}^L + vC_{11}^C + vC_{12}^C + v'C_{12}^L} + v'C_{13}^C + vC_{33}^L\right]S_3 - \left[\frac{2vv'(C_{13}^C - C_{13}^L)(C_{13}^L - C_{13}^C)}{v'C_{11}^L + vC_{11}^C + vC_{12}^C + v'C_{12}^L} + v'C_{13}^C + vC_{33}^L\right]E_3 \tag{5}$$

$$\overline{D_3} = \left[\frac{2vv'\left(e_{31}^C - e_{31}^L\right)\left(C_{13}^L - C_{13}^C\right)}{v'C_{11}^L + vC_{11}^C + vC_{12}^C + v'C_{12}^L} + v'e_{33}^C + ve_{33}^L\right]S_3 - \left[\frac{2vv'(C_{13}^C - C_{13}^L)(C_{13}^L - C_{13}^C)}{v'C_{11}^L + vC_{11}^C + vC_{12}^C + v'C_{12}^L} + v'\varepsilon_{11}^C + v\varepsilon_{33}^L\right]E_3 \tag{6}$$

The equation for displacement can be also expressed as shown in equation (7). We can then obtain the equation for the dielectric constant and is shown in equation (8).

$$\overline{D_3} = \overline{e_{33}}S_3 + \overline{\varepsilon_{33}^S}E_3 \tag{7}$$

$$\overline{\varepsilon_{33}^S} = \frac{2vv'(C_{13}^C - C_{13}^L)(C_{13}^L - C_{13}^C)}{v'C_{11}^L + vC_{11}^C + vC_{12}^C + v'C_{12}^L} + v'\varepsilon_{11}^C + v\varepsilon_{33}^L \tag{8}$$

We compared the derived dielectric constant using equation (8) against the measured value of the fabricated 1-3 composite material to prove the validity of the equation.

B. IPB COMPOSITE AND FABRICATION

Since the proposal of piezoelectric material in 1981, various composite structures, such as 0-3, 2-2, and 1-3 composite, and fabrication methods have been studied [17], [20]. The main purpose of the composite is to improve the performance of piezoelectric material by adjusting the volume fraction ratio of each component [30]. The most widely used method to make the composite structure is the dice-and-fill method, where several cuts are made to the piezoelectric layer to have a series of kerfs using the dicing saw and fill those kerfs with a filling epoxy. However, to make the LN-BT composite using the dice-and-fill method, since LN is already in a solid plate form, not only the BT needs to be uniformly mixed with epoxy, but also the BT-filled composite requires additional high-temperature and high-pressure sintering process. Such fabrication is very difficult and does not guarantee uniformity or high dielectric constant of LN-BT composite. The IPB fabrication method was developed to improve the volume fraction limitation of composite material caused by physical dicing of the dice-and-fill method [24], [25]. In this study, since there is no extreme fabrication condition in IPB fabrication method, we can develop the LN-BT composite that guarantees a high dielectric constant.

The LN and BT solid plates were prepared, and both plates were lapped down to the preset thickness by the lapping machine (PM6, Logitech Inc., U.K.). Appropriate kerfs were made by the dicing process (DAD 3240, DISCO Inc., Japan) depending on the pre-determined volume fraction ratio. After aligning the kerfs of both plates not to interfere with each other, we then combined both plates inter-digitally, as shown in Fig. 3 (a). The kerfs were filled the with epoxy (Epo-Tek 301, Epoxy Technology Inc., MA, U.S.A.), and the samples were cured at recommended temperature and humidity. While bonding, we applied constant pressure over plates by using weights and confirmed that consistent kerfs were generated between posts during bonding utilizing a microscope. After curing, the lapping down of top and bottom surfaces exposed the 2-2 composite structure, as shown in Fig. 3 (b). A new BT solid plate was then prepared and was diced in the same

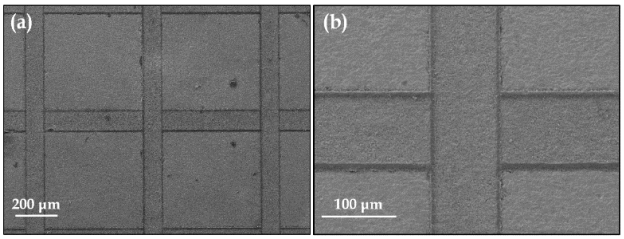

FIGURE 4. The SEM image for 1-3 IPB-based composite sample (a), expanded image (b).

manner after rotating 90°. Both diced plates were combined inter-digitally, as shown in Fig. 3 (c), and the kerfs were filled. After curing and lapping down the BT plate, 1-3 composite material was finished, as shown in Fig. 3 (d).

III. RESULTS AND DISCUSSION

We prepared 1-3 composite samples by using IPB with the LN volume fraction ratios of 50%, 60%, 70%, 80%, and 100%, as shown in Fig. 3 (d). By fixing the physical dimension of the composite samples at 8 mm x 8 mm x 0.3 mm, we set the dielectric constant as the only determining factor of the capacitance and observed the effect of different volume fraction ratios on the dielectric constant, the capacitance, subsequently to the electrical impedance. We confirmed that the finished composite had appropriate structure and connectivity using SEM images (VEGA3 SBH, TESCAN Inc., Czech) as shown in Fig. 4. In particular, the kerf between LN and BT, filled by epoxy, was confirmed to be evenly spaced over the entire sample, and samples have the same structure as designed in Fig. 3 (a).

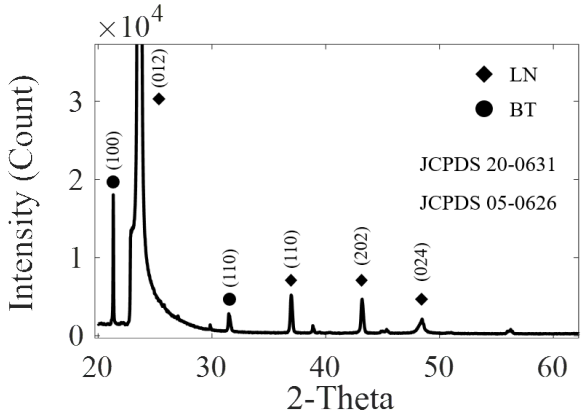

FIGURE 5. The graph of X-ray diffraction measurement result.

Although there are physical errors while dicing, the gaps between interdigitated solid-state plates were same, and the mechanical damages caused by the dicing process were minimized on the contact surface, as shown in Fig. 4. We performed XRD measurement for the fabricated LN-BT composite sample and obtained the XRD pattern from the area covering several LN pillars and BT inserts, as shown in Fig. 5. These findings confirm that the sample has a perovskite structure, and the IPB composite fabrication process was successful in combining two different materials, LN and BT. As per the standard JCPDS 20-0631, LN was generally identified in the appearance of XRD pattern at 24°, 33°, 35°, 40°, 43°, 48°, 53°, and 56° which corresponds to (012), (104), (110), (113), (202), (024), (116), and (122), respectively. Similarly, as per the standard JCPDS 05-0626, BT was identified in the appearance of XRD pattern at 22°, 31°, 39°, 45°, 51°, 56°, and 66° which corresponds to (100), (110), (111), (002), (210), (211) and (220), respectively. As shown Fig. 5, the diffraction peak shows that LN has trigonal structure and BT has tetragonal structure. However, since it is a composite structure, the peak is not very sharp and is slightly shifted.

The dielectric constant of fabricated samples was measured using an impedance analyzer (E4990A, Keysight Inc., CA, U.S.A.) at 1 kHz frequency. The measured and simulated results are graphed and compared in Fig. 6. To obtain the dielectric constant results for samples with various volume fraction ratio, we first measured the capacitance value using an impedance analyzer and then calculated the dielectric constant and physical values, such as thickness and aperture size. Based on equations between capacitance and dielectric constant and the reference material data in Table 2, we graphed the IPB composite simulation results in Fig. 6.

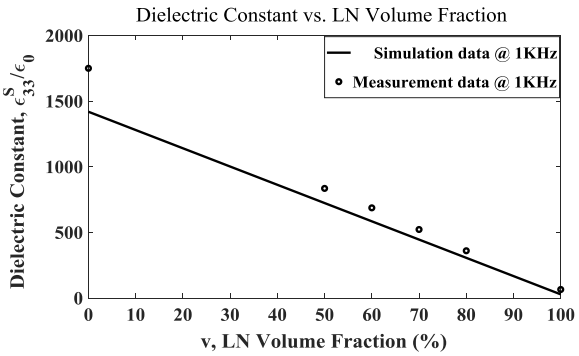

FIGURE 6. The graph for comparison between simulation result and measurement result. Measurement frequency: 1 KHz.

From Fig. 6, we can confirm that the distribution curve of the measured data and the simulation curve are similar. Previous studies show that the dielectric constant of the 0-3 composite by BT and polyimide was increased by 10 to 15 at the 80% volume fraction ratio [31], [32]. There was another case of increasing the dielectric constant by 20 from 0-3 composites of PVDF-TrFE and $CaCu_3Ti_4O_{12}$ [33]. The dielectric constant in our LN-BT composite was improved by about 300 at an 80% volume fraction compared to the LN plate. Our study also confirmed that the lower the volume fraction of LN, the higher the dielectric constant achievable and vice versa. Our proposed approach increased the dielectric constant significantly, and we believe the main reason is that the IPB method using a solid-state plate guarantees a high dielectric constant.

TABLE 2. Material properties for lithium niobate and barium titanate [22].

Materials	Elastic Compliance Constant (10^{-12} m^2/N)						Elastic stiffness Constant (10^{10} N/m^2)					
	$S^D{}_{11}$	$S^D{}_{12}$	$S^D{}_{13}$	$S^D{}_{33}$	$S^D{}_{44}$	$S^D{}_{66}$	$C^E{}_{11}$	$C^E{}_{12}$	$C^E{}_{13}$	$C^E{}_{33}$	$C^E{}_{44}$	$C^E{}_{66}$
$LiNbO_3$	5.2	-0.44	-1.45	4.89	10.8	11.3	2.03	0.573	0.752	2.424	0.595	0.728
$BaTiO_3$	8.18	-2.98	-1.95	6.76	18.3	22.3	16.6	7.66	7.75	16.2	4.29	4.48
	Piezoelectric Coefficient						Dielectric Constants					
	d_{33}	d_{31}	d_{15}	e_{33}	e_{31}	e_{15}	$\varepsilon^T{}_{33}$	$\varepsilon^T{}_{11}$	$\varepsilon^S{}_{33}$	$\varepsilon^S{}_{11}$		
$LiNbO_3$	6.0	-0.85	69.2	1.3	0.23	3.83	28.7	85.2	27.9	44.3		
$BaTiO_3$	191	-79	270	11.6	-4.4	18.6	1898	1622	1419	1269		

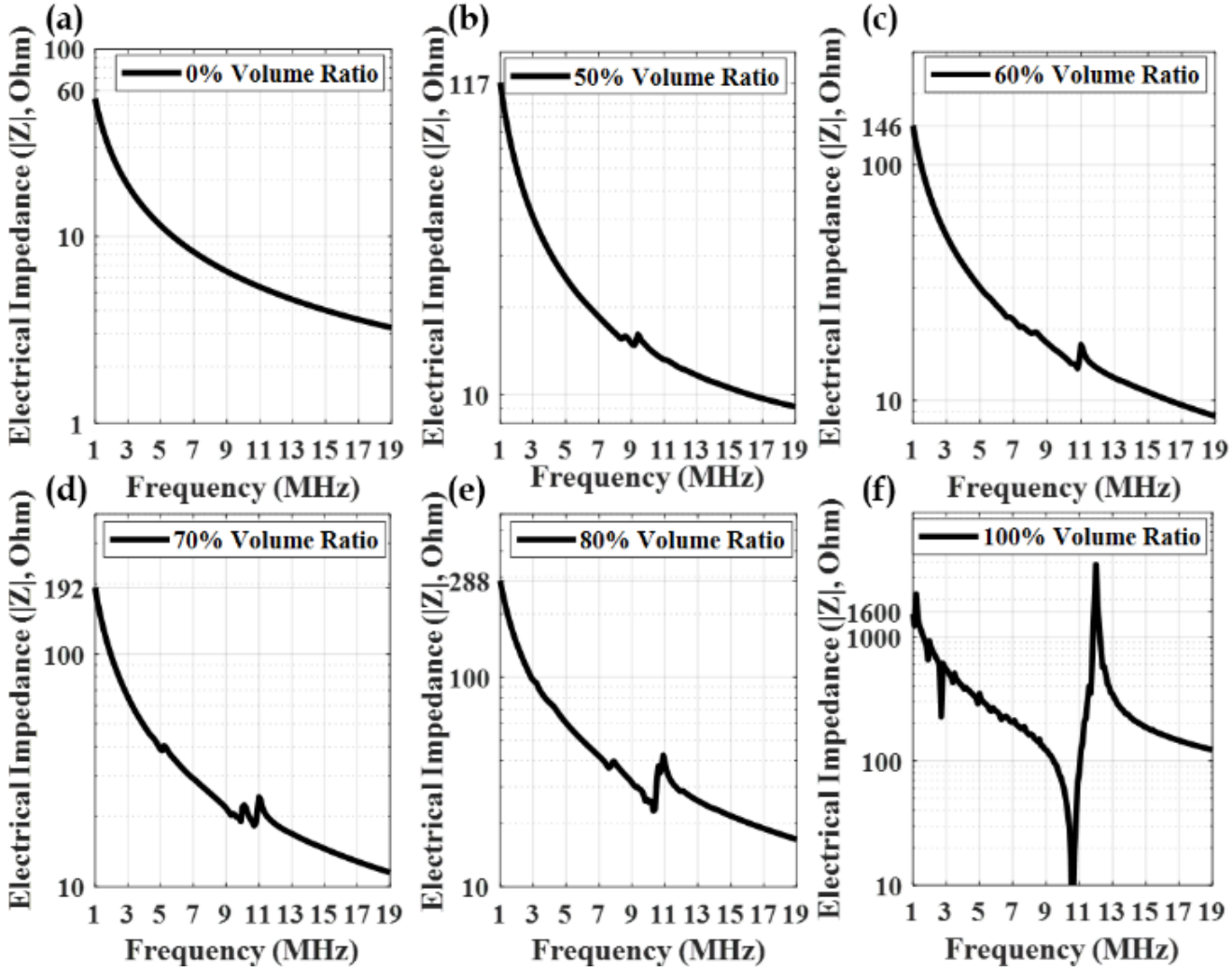

FIGURE 7. The measurement results for IPB-based composite sample and LN, and BTO samples. (a) BTO, (b) 50%, (c) 60%, (d) 70%, (e) 80% IPB-based composite sample, and (f) LN samples. The meaning of percentage is the volume fraction ratio occupied by LN to the volume of all samples.

We measured the electrical impedance of IPB composites having LN volume fraction ratios of 50%, 60%, 70%, 80%, and 100% and presented the results in Fig. 7. Comparing the electrical impedance magnitude at 1 MHz, which is the y-intercept of each graph, we can observe that the electrical impedance magnitude of the IPB composite sample is decreased as the volume fraction ratio of LN is reduced. It demonstrates that the electrical impedance we were targeting was considerably improved by creating a 1-3 composite with high-dielectric BT by IPB without changing the area and

thickness. We also obtained the series resonance frequency (f_s) and the parallel resonance frequency (f_p), which are frequencies corresponding to the minimum impedance magnitude and maximum impedance magnitude, respectively, from Fig. 7, and calculated the k_t with equation (9) [34]. The k_t for the LN volume fraction ratios of 100 %, 80 %, 70 %, 60 %, and 50 % were 0.48, 0.33, 0.23, 0.23, and 0.2, respectively, and we observed that the k_t value of IPB composite samples decreases as the LN volume fraction decreases. However, the k_t value can be improved by optimizing the aspect ratio of LN rods, which were not considered here.

$$k_t^2 = \frac{\left(f_p^2 - f_s^2\right)}{f_p^2} \tag{9}$$

In addition, to demonstrate that the lead component was not present in the IPB-based composite samples, EDS (X-act, Oxford Instruments Inc., U.K.) was used to analyze the included components in the samples. Table 3 shows the results for three randomly selected points for the sample in Fig. 4. Since the EDS equipped with a Beryllium (Be) window cannot measure materials lighter than sodium atom, the lithium atom, which is lighter than sodium atom, is not observed in Table 3. Combining with the XRD measurement results, it can be clearly seen that LN and BT are present in the sample, while the lead element is not.

TABLE 3. Components of IPB composite measured by EDS.

Item	Unit	Point 1	Point 2	Point 3
C (Carbon)	wt %	21	18	19
O (Oxygen)	wt %	22	24	23
Ti (Titanium)	wt %	5	4	4
Nb (Niobate)	wt %	33	44	40
Ba (Barium)	wt %	19	10	14
Total	wt %	100	100	100

One of the limitations of the designed composite is that the electromechanical coupling coefficients of fabricated samples in this study were low. However, this limitation can be overcome by optimizing the aspect ratio of LN rods and the spacing between the rods, which we will be addressing in a future study. In addition, The LN-BT composite results presented here can be extended to a variety of combinations of LN with other high dielectric constants materials, such as calcium copper titanate. In addition, we expect that the results of this study can be used in various applications. For example, it can be used for (a) acoustic actuators and ultrasonic motors using high Q_m, (b) miniaturized transducers using high-dielectric constant, and (c) pMUT (piezoelectric micromachined ultrasonic transducers) using MEMS fabrication process.

In this study, since the dicing saw was used for the patterning process, there was a physical limitation. However, when it is combined with the MEMS fabrication process, we expect that micro-patterns can be easily implemented, and the efficiency can be improved. The advantages of our composite, such as safety, compactness of packaging, and the piezoelectric efficiency of lead-free composite, lend themselves to several medical applications, such as miniaturized ultrasound transducers, implantable devices, and acoustic energy transfer.

IV. CONCLUSION

With the increase in regulations restricting lead, the demand for lead-free piezoelectric materials has been increasing. LN is a commonly used lead-free material. However, it is limited for miniaturization application due to its low dielectric constant and high electrical impedance. We overcome these limitations of LN with LN-BT modeling, based on ceramic composite modeling and IPB based composite. We used solid LN and BT plates to guarantee the high dielectric constant. We showed that the dielectric constant and electrical impedance of the IPB-based composite material was improved through analysis and results from the impedance analyzer. We also confirmed that the lead component was not included in IPB-based composite material by XRD and SEM-EDS measurements. Thus, we believe the proposed component would have a major role in designing lead-free miniaturized medical devices in the near future.

ACKNOWLEDGMENT

(Kyungmin Kim and Jinhee Yoo contributed equally to this work.)

REFERENCES

[1] European Union, *Directive 2002/95/EC of the European Parliament and of the Council of 27 January, 2003*, Brussels, Belgium, 2003.
[2] Y. Saito, H. Takao, T. Tani, T. Nonoyama, K. Takatori, T. Homma, T. Nagaya, and M. Nakamura, "Lead-free piezoceramics," *Nature*, vol. 432, no. 7013, pp. 84–87, 2004.
[3] Y. Zhang and J.-F. Li, "Review of chemical modification on potassium sodium niobate lead-free piezoelectrics," *J. Mater. Chem. C*, vol. 7, no. 15, pp. 4284–4303, 2019.
[4] X. Yan, K. H. Lam, X. Li, R. Chen, W. Ren, X. Ren, Q. Zhou, and K. K. Shung, "Correspondence: Lead-free intravascular ultrasound transducer using BZT-50BCT ceramics," *IEEE Trans. Ultrason., Ferroelectr., Freq. Control*, vol. 60, no. 6, pp. 1272–1276, Jun. 2013.
[5] L. Qiao, G. Li, H. Tao, J. Wu, Z. Xu, and F. Li, "Full characterization for material constants of a promising KNN-based lead-free piezoelectric ceramic," *Ceram. Int.*, vol. 46, no. 5, pp. 5641–5644, Apr. 2020.
[6] Z. Zhang, R. Chen, B. Wang, T. Zhang, M. Su, R. Liu, J. Yang, X. Cao, Y. Li, H. Zheng, K. K. Shung, M. S. Humayun, Q. Zhou, and W. Qiu, "Development of a KNN ceramic-based lead-free linear array ultrasonic transducer," *IEEE Trans. Ultrason., Ferroelectr., Freq. Control*, vol. 65, no. 11, pp. 2113–2120, Nov. 2018.
[7] M. Xia, C. Luo, X. Su, Y. Li, P. Li, J. Hu, G. Li, H. Jiang, and W. Zhang, "KNN/PDMS/C-based lead-free piezoelectric composite film for flexible nanogenerator," *J. Mater. Sci., Mater. Electron.*, vol. 30, no. 8, pp. 7558–7566, Apr. 2019.
[8] T. Shao, H. Du, H. Ma, S. Qu, J. Wang, J. Wang, X. Wei, and Z. Xu, "Potassium–sodium niobate based lead-free ceramics: Novel electrical energy storage materials," *J. Mater. Chem. A*, vol. 5, no. 2, pp. 554–563, 2017.

[9] J. Wu, "Perovskite lead-free piezoelectric ceramics," *J. Appl. Phys.*, vol. 127, no. 19, May 2020, Art. no. 190901.

[10] R. S. Weis and T. K. Gaylord, "Lithium niobate: Summary of physical properties and crystal structure," *Appl. Phys. A Solids Surf.*, vol. 37, no. 4, pp. 191–203, Aug. 1985.

[11] M. Zhang, C. Wang, R. Cheng, A. Shams-Ansari, and M. Lončar, "Monolithic ultra-high-*Q* lithium niobate microring resonator," *Optica*, vol. 4, no. 12, pp. 1536–1537, 2017.

[12] J. Lin, Y. Xu, Z. Fang, M. Wang, J. Song, N. Wang, L. Qiao, W. Fang, and Y. Cheng, "Fabrication of high-*Q* lithium niobate microresonators using femtosecond laser micromachining," *Sci. Rep.*, vol. 5, no. 1, pp. 1–4, Jul. 2015.

[13] M. R. H. Sarker, H. Karim, R. Martinez, N. Love, and Y. Lin, "A lithium niobate high-temperature sensor for energy system applications," *IEEE Sensors J.*, vol. 16, no. 15, pp. 5883–5888, Aug. 2016.

[14] S. Zhang, J. B. Lim, H. J. Lee, and T. R. Shrout, "Characterization of hard piezoelectric lead-free ceramics," *IEEE Trans. Ultrason., Ferroelectr., Freq. Control*, vol. 56, no. 8, pp. 1523–1527, Aug. 2009.

[15] K.-K. Wong, *Properties of Lithium Niobate*, vol. 28. Edison, NJ, USA: IET, 2002.

[16] A. Baba, C. T. Searfass, and B. R. Tittmann, "High temperature ultrasonic transducer up to 1000 °C using lithium niobate single crystal," *Appl. Phys. Lett.*, vol. 97, no. 23, Dec. 2010, Art. no. 232901.

[17] R. E. Newnham, L. J. Bowen, K. A. Klicker, and L. E. Cross, "Composite piezoelectric transducers," *Mater. Des.*, vol. 2, no. 2, pp. 93–106, 1980.

[18] W. A. Smith and B. A. Auld, "Modeling 1–3 composite piezoelectrics: Thickness-mode oscillations," *IEEE Trans. Ultrason., Ferroelectr., Freq. Control*, vol. 38, no. 1, pp. 40–47, Jan. 1991.

[19] K. C. Cheng, H. L. W. Chan, C. L. Choy, Q. Yin, H. Luo, and Z. Yin, "Single crystal PMN-0.33 PT/epoxy 1–3 composites for ultrasonic transducer applications," *IEEE Trans. Ultrason., Ferroelectr., Freq. control*, vol. 50, no. 9, pp. 1177–1183, Sep. 2003.

[20] S. Dash, R. N. P. Choudhary, and M. N. Goswami, "Enhanced dielectric and ferroelectric properties of PVDF-$BiFeO_3$ composites in 0–3 connectivity," *J. Alloys Compounds*, vol. 715, pp. 29–36, Aug. 2017.

[21] W. A. Smith, "Modeling 1–3 composite piezoelectrics: Hydrostatic response," *IEEE Trans. Ultrason., Ferroelectr., Freq. Control*, vol. 40, no. 1, pp. 41–49, Jan. 1993.

[22] D. Xue, Y. Zhou, H. Bao, C. Zhou, J. Gao, and X. Ren, "Elastic, piezoelectric, and dielectric properties of $Ba(Zr_{0.2}Ti_{0.8})O_3$-$50(Ba_{0.7}Ca_{0.3})TiO_3$ Pb-free ceramic at the morphotropic phase boundary," *J. Appl. Phys.*, vol. 109, no. 5, Mar. 2011, Art. no. 054110.

[23] A. W. Warner, M. Onoe, and G. A. Coquin, "Determination of elastic and piezoelectric constants for crystals in class (3*m*)," *J. Acoust. Soc. Amer.*, vol. 42, no. 6, pp. 1223–1231, 1967.

[24] R. Liu, K. A. Harasiewicz, and F. S. Foster, "Interdigital pair bonding for high frequency (20–50 MHz) ultrasonic composite transducers," *IEEE Trans. Ultrason., Ferroelectr., Freq. Control*, vol. 48, no. 1, pp. 299–306, Jan. 2001.

[25] J. M. Cannata, J. A. Williams, L. Z. Zhang, C. H. Hu, and K. K. Shung, "A high-frequency linear ultrasonic array utilizing an interdigitally bonded 2–2 piezo-composite," *IEEE Trans. Ultrason., Ferroelectr., Freq. Control*, vol. 58, no. 10, pp. 2202–2212, Oct. 2011.

[26] S. Sanna and W. G. Schmidt, "Lithium niobate *X*-cut, *Y*-cut, and *Z*-cut surfaces from *ab initio* theory," *Phys. Rev. B, Condens. Matter*, vol. 81, no. 21, p. 214116, 2010.

[27] N. Schmarje, K. J. Kirk, and S. Cochran, "Comparison of y/36°-cut and *z*-cut lithium niobate composites for high temperature ultrasonic applications," *Nondestruct. Test. Eval.*, vol. 20, no. 2, pp. 77–87, 2005.

[28] H. Ogi, Y. Kawasaki, M. Hirao, and H. Ledbetter, "Acoustic spectroscopy of lithium niobate: Elastic and piezoelectric coefficients," *J. Appl. Phys.*, vol. 92, no. 5, pp. 2451–2456, Sep. 2002.

[29] R. S. Cobbold, *Foundations of Biomedical Ultrasound*. London, U.K.: Oxford Univ. Press, 2006, pp. 336–342.

[30] H. P. Savakus, K. A. Klicker, and R. E. Newnham, "PZT-epoxy piezoelectric transducers: A simplified fabrication procedure," *Mater. Res. Bull.*, vol. 16, no. 6, pp. 677–680, Jun. 1981.

[31] S.-H. Xie, B.-K. Zhu, X.-Z. Wei, Z.-K. Xu, and Y.-Y. Xu, "Polyimide/$BaTiO_3$ composites with controllable dielectric properties," *Compos. A, Appl. Sci. Manuf.*, vol. 36, no. 8, pp. 1152–1157, Aug. 2005.

[32] S. Yue, B. Wan, Y. Liu, and Q. Zhang, "Significantly enhanced dielectric constant and energy storage properties in polyimide/reduced $BaTiO_3$ composite films with excellent thermal stability," *RSC Adv.*, vol. 9, no. 14, pp. 7706–7717, 2019.

[33] L. Zhang, X. Shan, P. Bass, Y. Tong, T. D. Rolin, C. W. Hill, J. C. Brewer, D. S. Tucker, and Z.-Y. Cheng, "Process and microstructure to achieve ultra-high dielectric constant in ceramic-polymer composites," *Sci. Rep.*, vol. 6, no. 1, pp. 1–10, Dec. 2016.

[34] Q. Chen and Q.-M. Wang, "The effective electromechanical coupling coefficient of piezoelectric thin-film resonators," *Appl. Phys. Lett.*, vol. 86, no. 2, Jan. 2005, Art. no. 022904.

KYUNGMIN KIM (Graduate Student Member, IEEE) received the B.S. degree in electronic engineering from Kyungpook National University, South Korea, in 2016. He is currently pursuing the M.S.-Ph.D. degree with the Convergence IT Engineering Department, POSTECH, South Korea. His research interests include piezoelectric material, MEMS, piezoelectric micromachined ultrasonic transducer (pMUT), device fabrication, and signal processing.

JINHEE YOO (Graduate Student Member, IEEE) received the B.S. degree in electrical and computer engineering from Ajou University, Suwon, South Korea, in 2018. He is currently pursuing the Integrated M.S. and Ph.D. degree with the School of Interdisciplinary Bioscience and Bioengineering, Pohang University of Science and Technology, Pohang, South Korea. His current research interests include medical imaging using high frequency ultrasound and biomedical application with acoustic tweezers.

HAE GYUN LIM received the B.S. degree in biochemistry from the University of California, Los Angeles, Los Angeles, CA, USA, in 2010, and the M.S. and Ph.D. degrees in biomedical engineering from the University of Southern California, Los Angeles, in 2014 and 2017, respectively. From 2013 to 2017, he was a Research Assistant with the NIH Resource Center for Medical Ultrasonic Transducer Technology. He worked as a Research Assistant Professor with the Future IT Innovation Laboratory, Pohang University of Science and Technology (POSTECH), Pohang, South Korea, until 2020. He is currently an Assistant Professor with the Department of Biomedical Engineering, Pukyong National University, Busan, South Korea. His research interests include ultrasonic transducers, cell mechanics, HIFU treatment, ultrasound imaging, and high frequency ultrasound microbeams.

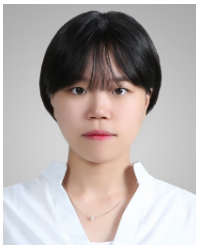

MINA LEE received the B.S. degree in mechanical engineering and the M.S. degree in convergence IT engineering from the Pohang University of Science and Technology (POSTECH), Pohang, South Korea, in 2017 and 2021, respectively. Her current research interests include soft actuators, soft sensors, soft robotics, biomedical applications, and mechanics of materials.

SUNG-MIN PARK (Member, IEEE) received the B.S. and Ph.D. degrees in electrical and computer engineering from Purdue University, West Lafayette, IN, USA, in 2001 and 2006, respectively. He is currently a Professor with the Department of Convergence IT Engineering, the Department of Electrical Engineering, and the Department of Mechanical Engineering, Pohang University of Science and Technology (POSTECH), Pohang, South Korea, and the School of Interdisciplinary Bioscience and Bioengineering, POSTECH. He has been with POSTECH, since 2016. From 2006 to 2014, he was with Medtronic, Minneapolis, MN, USA, as a Research and Development Manager, leading the award-wining effort in developing the world first MRI conditional pacemaker. From 2014 to 2016, he was with Samsung, Suwon, South Korea, as the Director, spearheading healthcare centric mobile device and mobile health service platform development projects.

HYUNG HAM KIM (Member, IEEE) received the B.S. degree in electrical engineering from the Korea Advanced Institute of Science and Technology, Daejeon, South Korea, in 1993, the M.S. degree in electrical engineering from Seoul National University, Seoul, South Korea, in 1995, and the M.S. and Ph.D. degrees in biomedical engineering from the University of Southern California, Los Angeles, CA, USA, in 2006 and 2010, respectively. He was the Manager and a Principal Engineer with the Probe Department, Medison Company Ltd., Seoul, from 1994 to 2004, where he managed the research and development projects of medical ultrasound array transducers. He was a Research Assistant Professor with the Department of Biomedical Engineering, University of Southern California, where he was also the Manager of the NIH Resource Center for Medical Ultrasonic Transducer Technology. He joined Analogic Inc., Peabody, MA, USA, in 2014, where he led the research solutions business as the Director of Business Development, until 2016. He is currently an Associate Professor with the Department of Convergence IT Engineering and the Department of Electrical Engineering, Pohang University of Science and Technology (POSTECH), Pohang, South Korea, and the School of Interdisciplinary Bioscience and Bioengineering, POSTECH. His current research interests include high frequency array transducers for high resolution ultrasound imaging, cellular mechanics studies using high frequency ultrasound, and neuromodulation using focused ultrasound.